K-INFINITY BENCHMARK EXPERIMENTS IN INTERMEDIATE NEUTRON SPECTRA FOR VARIOUS STRUCTURAL MATERIALS

Anatoli Tsiboulia, Mark Nikolaev, Vladimir Golubev, Yevgeniy Rozhikhin
Institute of Physics and Power Engineering
1 Bondarenko Sq., Obninsk, Kaluga Region 249020, Russian Federation,
abbn@ippe.obninsk.ru

Virginia F. Dean
Consultant to Idaho National Engineering and Environmental Laboratory
HC 1 Box 407, Elgin, Arizona 85611, United States of America
vfdean@aol.com

ABSTRACT

Experiments designed for the estimation of k_∞ of compositions of highly enriched uranium and such structural materials of nuclear reactors as iron, chromium, nickel, zirconium, and molybdenum are described in this report. A description of the experimental method is given. Results of reactivity-worth measurements in combination with calculations were used to determine k_∞ of the benchmark model of the experiments. Results of calculations of the benchmark model of the experiments are presented.

1. INTRODUCTION

Several k_∞ experiments were performed in the 1970's-80's at the COBRA critical facility at the Institute of Physics and Power Engineering (IPPE), Obninsk, Russian Federation. The experimental program consisted of determination of k_∞ for combinations of highly enriched (90% ^{235}U) uranium dioxide with various structural materials: nickel (KBR-7 assembly), stainless steel (KBR-9), stainless steel and molybdenum (KBR-10), chromium (KBR-15), and zirconium (KBR-16).

All five of these experiments were evaluated and accepted for the *International Handbook of Evaluated Criticality Safety Benchmark Experiments*[1] (HEU-COMP-INTER-005).

2. DESCRIPTION OF EXPERIMENTAL CONFIGURATIONS

2.1 OVERVIEW OF THE FACILITY

The COBRA critical facility is a large set of a stainless steel tubes (5.0 cm in outer diameter, 0.1 cm wall thickness, and about 160 cm long) supported by a stainless steel plate. The plate lies on four horizontal steel angle bars fastened on four vertical steel channels. The distance between the room floor and the support plate is 200 cm. The support plate with diameter 230 cm and thickness 13 cm had 1400 holes 1.8 cm in diameter to fix the positions of the tubes containing fissile and structural materials. The pitch of the hexagonal lattice of these holes was 5.1 cm. The control and safety rod drivers were located below the support plate.

The whole facility construction was placed in the center of a reactor room with dimensions $12 \times 6 \times 7$ m. The concrete walls of this room had thickness of about 1 m.

2.2 DESIGN OF THE ASSEMBLIES

Each assembly had the test region at its center. Tubes in that region were filled with pellets of the investigated structural material with enriched uranium dioxide pellets added to provide k_{∞} of that region close to unity. The dimensions of the test region were so large that in the center part of this region the neutron spectrum was determined mainly by the neutron properties of that region.

The test region was surrounded on all sides by a driver region. The tubes in that region were filled with pellets of enriched uranium metal or dioxide mixed with pellets of stainless steel or graphite. The composition and thickness of the driver region was adjusted to provide criticality to the whole assembly.

Around the driver region was the reflector region. In all cases the tubes in the reflector region were filled with pellets of depleted-uranium dioxide. The side reflector was no smaller than 40 cm in thickness; the thickness of the top and bottom reflectors was about 30 cm.

An additional spectrum-adjusting buffer region was located between the driver region and test region in some assemblies (KBR-7, -15, and -16). This intermediate region contained structural material (not necessarily the same as in the test region) and fuel (KBR-15, -16) or only structural material (KBR-7).

2.3 THE FUEL AND REFLECTOR TUBES

The critical assemblies were built on the support plate from the steel tubes filled with cylindrical pellets of fissile, structural, and reflector materials. Contents of the fuel tubes is described in more detail below. The protuberances on the bottom of these tubes were put inside the holes of the support plate and were fixed by screws. The tops of the tubes were closed with special steel plugs. A spring under the top plug prevented the possibility of vertical displacement of the pellets inside the tubes. The upper parts of the tubes were connected with one another by special steel plates to fix the distance between the tubes installed in the hexagonal lattice.

2.4 THE CONTROL AND SAFETY RODS

Control and safety rod tubes were not fixed in the support plate but could freely move up and down through holes in the plate. The set of pellets in the control or safety rods was the same as in the neighboring fuel rods. In the normal upper positions, the safety rods were in exactly the same positions as these neighbor rods. In alarm situations the electromagnetic connectors of the safety rods would switch off, and the rods would fall down of their own weight and stop the chain reaction.

2.5 ASSEMBLY REGION UNIT CELLS

Each region of each assembly was filled with cells formed from tubes and the pellets enclosed in these tubes. The test-region unit cells of all assemblies are shown in Figure 1. Material data and dimensions of all structural elements of the test-region cells are given in Section 3. The whole thickness of the unit cell is equal to sum of the thicknesses of pellets which filled this cell.

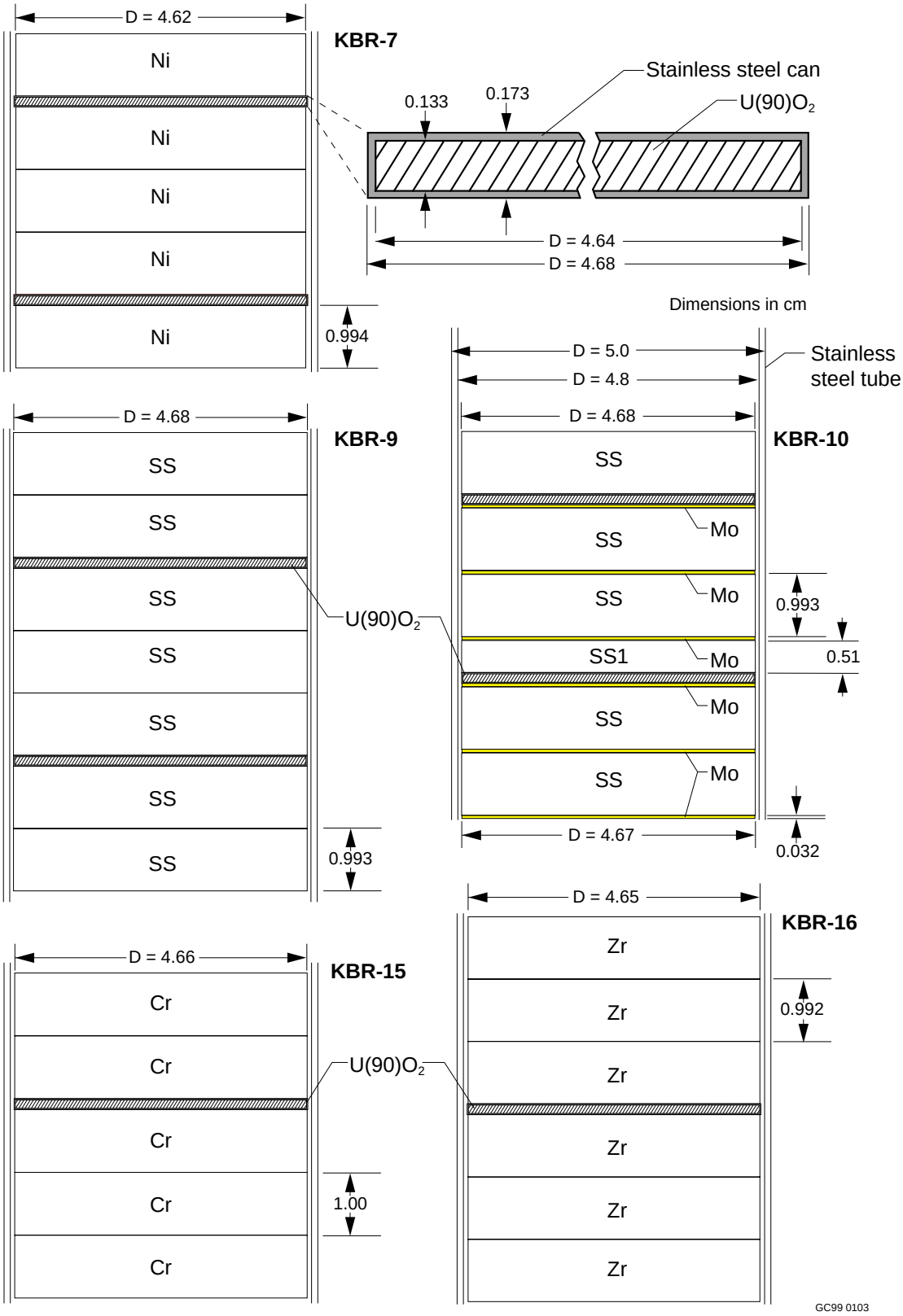

Figure 1. Composition of Test-Region Unit Cells of Critical Assemblies KBR-7, -9, -10, -15, and -16.

2.6 EXPERIMENTAL METHOD

The cell composition of every test region was chosen so that its k_∞ was not very different from unity. The geometry of each assembly was strongly symmetrical. The symmetry of the neutron flux in the vicinity of the central cell was confirmed by measurements of distributions of the ^{235}U and ^{238}U fission rates. So no corrections of the neutron current through the central cell were necessary.

The tube containing the central cell was longer than its neighbors. That tube was joined to the pneumatic driver of the reactor oscillator and could move up and down. A window was made in the wall of this tube at the location of the central cell. A thin cylindrical stainless steel container was inserted in the moveable tube through this window. The height of the container was greater than the maximum length of the cell. The upper and lower pellets of structural materials inside the container and the pellets of structural materials immediately above and below the container were adjusted (made thinner) so that the lattice regularity was preserved. Thus the only distortion of the lattice caused by the container in the center tube was the small increase of the amount of stainless steel around the central cell. Using the KBR-7 assembly, an attempt to measure the influence of this distortion on the measured reactivity worths was made, but no noticeable effect was found. This was confirmed also by calculations (see Section 4).

When the center tube was in its lower position, the container was exactly at the center of assembly. In its upper position, at the center of assembly was the usual central-region cell (and the part of the tube holding the container was above the core). In both positions, the contents of the center tube outside the container and within the core matched the contents of surrounding cells. The reactivity effect obtained by oscillation of the tube with a fully filled container was considered as background.

Four basic types of reactivity measurements were done:

- the reactivity measurement of replacing the lower part of the center tube with the upper part with the container with central cell (**background measurements**);
- the reactivity measurement of replacing the lower part of the center tube with the upper part with the container without the central cell (ρ_{cell} **measurements**);
- the reactivity measurement of replacing the lower part of the center tube with the upper part with the container without fuel (ρ_{fuel} **measurements**);
- the reactivity measurement of replacing the lower part of the center tube with the upper part with the container with fuel (or other cell components) replaced with stainless steel pellets (**correction measurements**).

(See Section 4 for more details.)

2.7 RESULTS OF REACTIVITY-WORTH MEASUREMENTS

Results of reactivity-worth measurements are given in Table I. Data are corrected for small deviations of weight of fuel and structural material in the experimental cell from average ones.

Cited uncertainties of reactivity measurements were estimated from the scattering of the results of independent measurements and then slightly increased to take into account uncertainties caused by correction for the stainless steel wall.

Table I. Reactivity-Worth Measurements.

Assembly	KBR-7	KBR-9	KBR-10	KBR-15	KBR-16
Investigated Material	Nickel	Stainless Steel	Stainless Steel & Molybdenum	Chromium	Zirconium
ρ_{fuel}, cents	0.423 ± 0.001	0.466 ± 0.001	0.435 ± 0.002	0.176 ± 0.002	0.1630 ± 0.0010
ρ_{cell}, cents	0.032 ± 0.002	0.069 ± 0.002	0.034 ± 0.002	0.057 ± 0.002	0.0095 ± 0.0015
$\rho_{cell} / \rho_{fuel}$	0.076 ± 0.005	0.148 ± 0.004	0.078 ± 0.004	0.324 ± 0.010	0.058 ± 0.006

3. DESCRIPTION OF MATERIAL DATA

The detailed composition data for test-region materials are listed in Table II.

The pellets used for reactivity measurements were weighed with high precision. The results of the reactivity worth measurements were corrected for the difference between the weight of the pellet used for the measurement and the weight of the "average" pellet. The uncertainties of the measured reactivities include the effect of the uncertainties of the weights and dimensions of the pellets used for these measurements (see Section 4).

Table II. Material Descriptions.

Pellet Identity	Dimensions and Mass	Nuclide	Wt.%
Uranium Dioxide	Diameter = 4.64 cm Thickness = 0.133 cm Mass = 15.000 g	^{235}U ^{238}U O	79.21 ± 0.11 8.69 12.10 ± 0.10
Stainless Steel Can around the Uranium Dioxide	Diameter = 4.68 cm Thickness = 0.02 cm Mass = 5.78 g	Fe Cr Ni Mn Ti Si C	69.8 17.6 ± 0.4 10.2 ±○ 0.3 1.2 ± 0.3 0.6 ± 0.1 0.5 ± 0.2 0.1 ± 0.05
Stainless Steel Pellets	Diameter = 4.68 cm Thickness = 0.993 cm [a] Mass = 132.6 g	Fe Cr Ni Mn Ti Si C	69.8 17.6 ± 0.4 10.2 ± 0.3 1.2 ± 0.3 0.6 ± 0.1 0.5 ± 0.2 0.1 ± 0.05
Stainless Steel Tube	OD = 5.00 cm Wall thickness = 0.1 cm Mass of 1 cm = 12.52 g	Fe Cr Ni Mn Ti Si C	69.8 17.6 ± 0.4 10.2 ± 0.3 1.2 ± 0.3 0.6 ± 0.1 0.5 ± 0.2 0.1 ± 0.05
Zirconium Pellet	Diameter = 4.65 cm Thickness = 0.992 cm Mass = 107.5 g	Zr Hf H	99.9553 0.040 ± 0.05 0.0047 ± 0.0009
Molybdenum Pellet	Diameter = 4.67 cm Thickness = 0.032 cm Mass = 5.50 g	Mo	100.0
Nickel Pellet	Diameter = 4.62 cm Thickness=0.994 cm Mass = 147.8 g	Ni Co	99.90 0.10 ± 0.05
Chromium Pellet	Diameter = 4.66 cm Thickness = 1.00 cm Mass = 103.1 g	Cr Fe Si O	99.23 0.16 ± 0.01 0.35 ± 0.01 0.26 ± 0.01

[a] In KBR-10, stainless steel pellets with thickness of 0.51 cm (SS1) were also used. (See Figure 1.)

4. DETAILED DESCRIPTION OF ASSEMBLIES

As was mentioned, the cores of all critical assemblies under consideration were designed as central subcritical test zones, or regions, surrounded by driver zones which ensured the critical condition of the whole assembly. In some assemblies, intermediate zones of structural material were placed between test zone and driver. In this section the structure of different zones' unit cells and construction of fuel rods, i.e. distribution of these unit cells inside of the stainless steel tubes, are shown.

The layout of fuel rods on the support plate of the facility are represented also. Only the central part of the whole assembly is shown in these layouts. The whole layout contains more depleted-UO_2 reflector rods, with 23 rods on each side of the complete hexagon (132 reflector rods in the outer rows).

Each fuel pellet was canned in aluminum or stainless steel. The parameters of fuel pellets used in the driver and reflector are shown in Table III.

Table III. Composition of Fuel Pellets Used in the Driver Zones and Reflector.

Pellet	Location	Can	Pellet Dia-meter, cm	Pellet Thick-ness, cm	Can Thick-ness, cm	Pellet Weight, g	Can Weight, g	Wt.%		
								^{235}U	^{238}U	O
U(90) metal	Core	Al	4.60	0.50	0.03	148.20	3.50	89.3	10.7	-
U(36) metal	Core	Al	4.60	0.50	0.03	148.17	3.50	36.3	63.7	-
$U(36)O_2$ (thick)	Core	SS	4.60	0.50	0.03	67.94	10.0	31.7	56.3	11.9
$U(36)O_2$ (thin)	Core	SS	4.64	0.133	0.02	15.00	5.75	31.8	56.1	12.1
$U(dep)O_2$	Reflector	Al	4.60	0.915	0.03	139.26	4.1	0.37	87.4	12.2

Additionally, pellets of stainless steel X28 were used in the driver zones of the KBR-9 and KBR-10 assemblies and in the intermediate zone of the KBR-15 assembly. Graphite pellets were used in all the assemblies' driver zones except that of KBR-7. The averaged parameters of these pellets are shown in Table IV.

Table IV. Parameters of X28 and C (Graphite) Pellets.

Pellets	Dimensions and weight	Nuclide	Weight %
X28	Diameter = 4.68 cm Thickness = 0.993 cm Weight = 127.58 g	Fe	71.1
		Cr	28.0
		Mn	0.35
		Si	0.40
		Ti	0.10
		C	0.05
C	Diameter = 4.68 cm Thickness = 0.993 cm Weight = 27.6 g	C	100.0

Characteristics of the remaining pellets used in the assemblies can be found in Section 3.

As mentioned in Section 2.6, a cylindrical stainless steel container in the longer center tube held the central cell of the assembly. The height of the container was 8 cm. The side wall of the container was 0.3 cm thick; the bottom and top stainless steel lids were 0.48 cm thick. To determine ρ_{fuel} the experimenters removed $U(90)O_2$ pellets. To determine ρ_{cell} they used measurements of reactivity from removing a unit cell. The pneumatic oscillator was used to quickly move the center tube from one position to the other ("rod-drop" method). Thin-walled stainless steel rings were inserted to maintain the position of the void in the inserted container. The measured reactivities ρ_{cell} and ρ_{fuel} were corrected for the extra amount of stainless steel around the cell or fuel that was present during the reactivity measurements. The amount of the correction was determined by reactivity measurements of stainless steel in the central cell.

KBR-7 ASSEMBLY

The KBR-7 assembly was designed as a quasi-spherical system with a central test zone, an intermediate zone of nickel pellets, and a driver zone, which consisted of pellets of metal uranium and uranium dioxide of different enrichments. Parameters of all pellets used in this assembly are shown in Tables II and III.

In Figure 2 the fuel rod structures are represented. The number of unit cells and pellets in different zones for each tube are shown here, as well as rod identification numbers (NN) and number of rods (quantity) used in the assembly.

There were small differences in the total heights for the different types of the rods. The rods were centered with respect to the horizontal midplane of the assembly during the tube-loading process. The total height of a set of pellets prepared for loading into the tube was measured, and a few stainless steel pellets were added to the bottom of the pellet set to adjust the midplane. The adjustment precision was ± 0.1 cm.

The layout of fuel tubes in the KBR-7 assembly is seen in Figure 3.

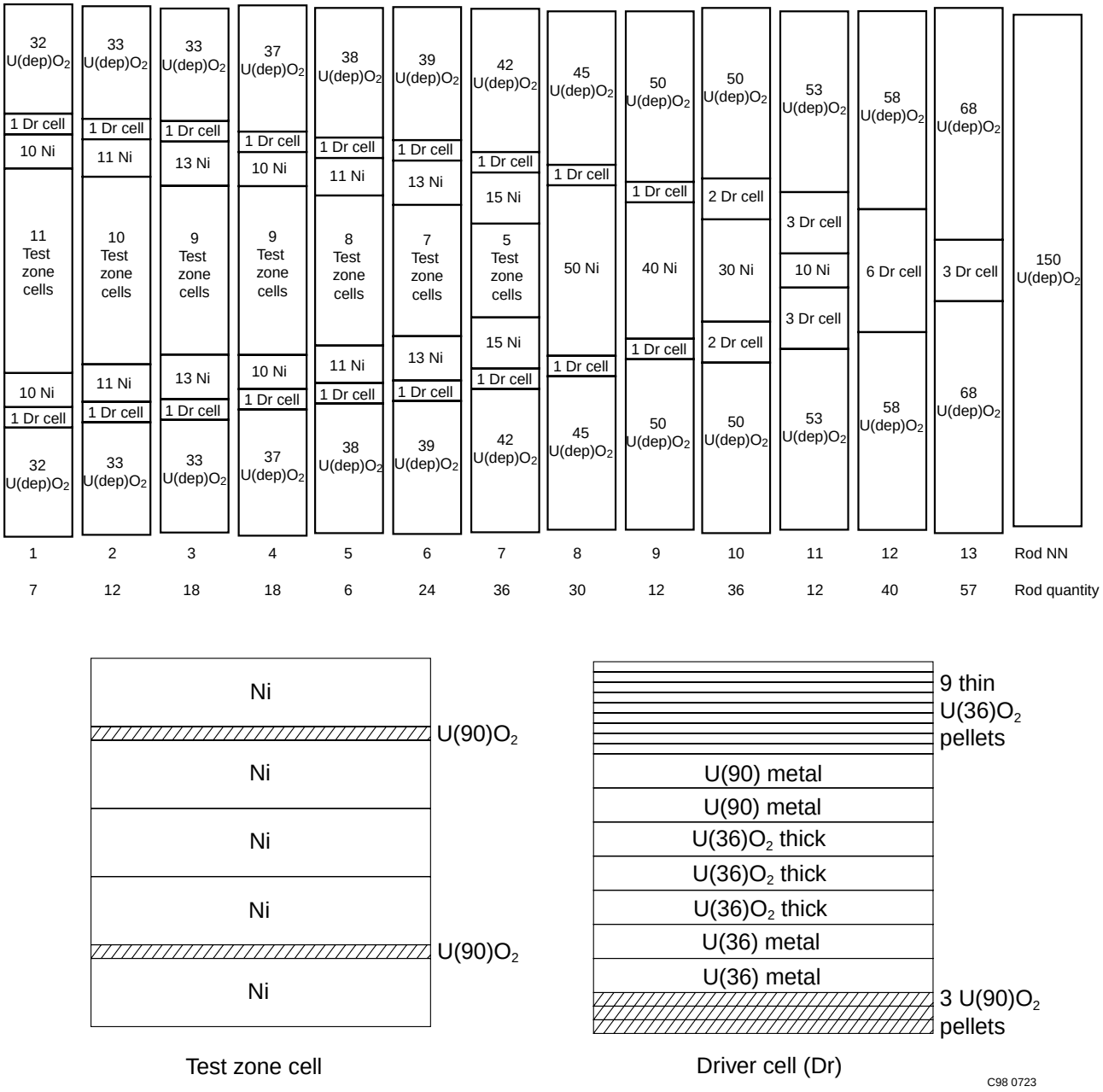

Figure 2. Rod Loading Scheme and Unit Cells of the KBR-7 Assembly.

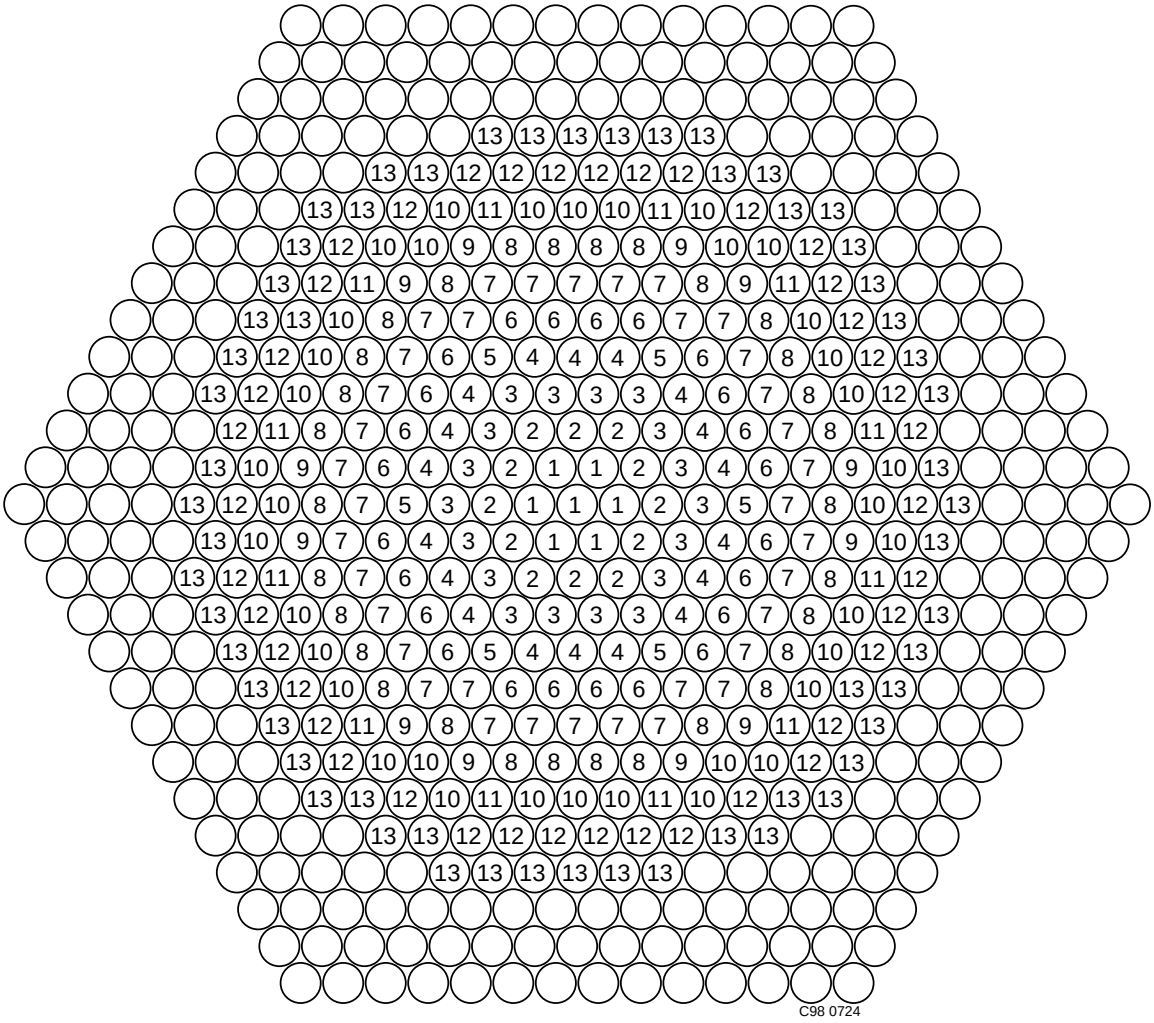

Figures inside circles correspond to the identification numbers of fuel tubes (NN).
Circles without numbers are the rods of the side reflector.

Figure 3. The Layout of the KBR-7 Assembly.

KBR-9 ASSEMBLY

This assembly was constructed as a quasi-cylindrical system. All the rods of the test zone consisted of the test-zone cells, driver cells, and depleted-uranium dioxide pellets as upper and lower reflector. Compositions of test-zone and driver unit cells and the loading of different rods are shown in Figure 4. In Figure 5 the layout of the assembly is shown.

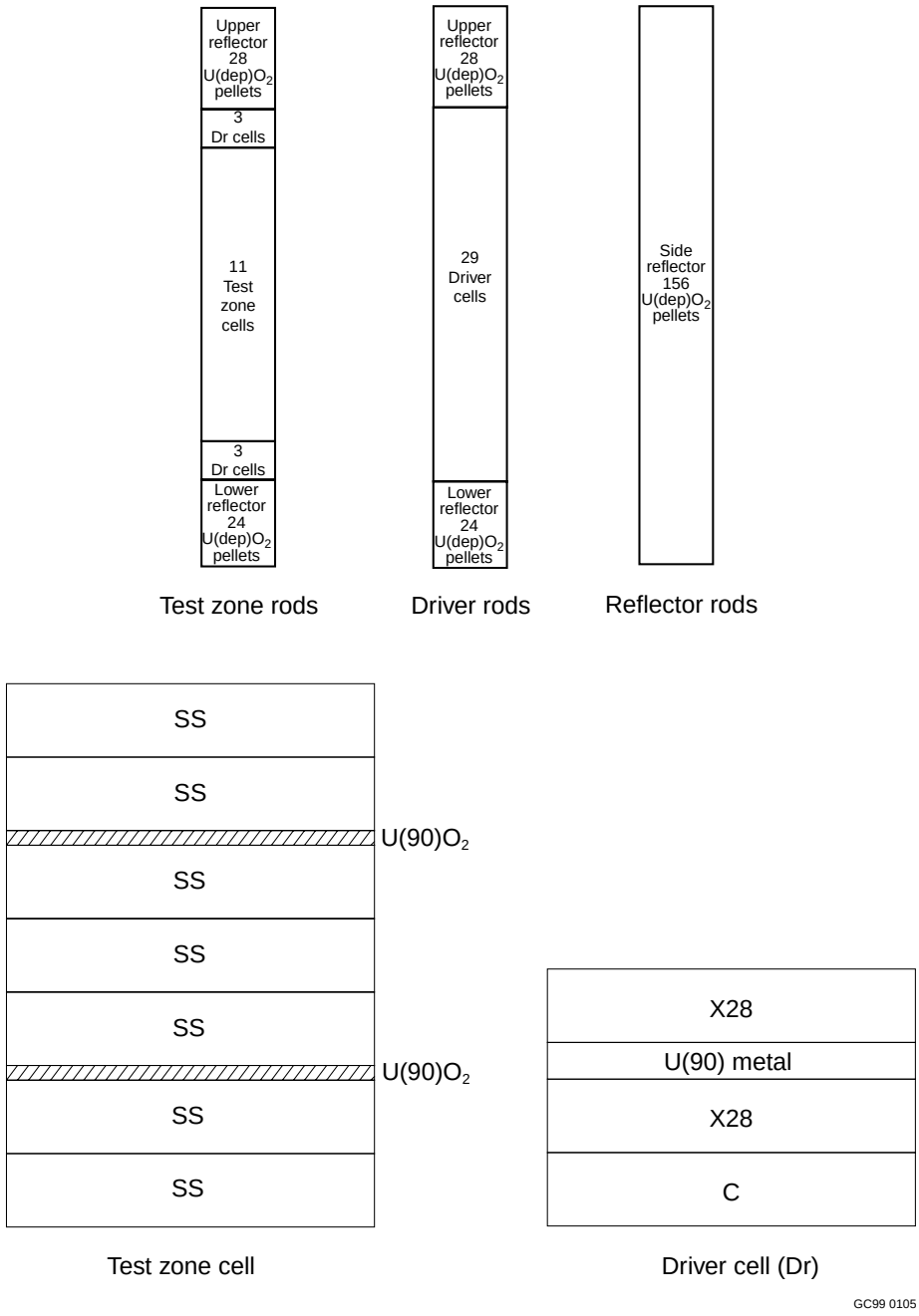

Figure 4. Rods and Cells in the Various Zones of the KBR-9 Assembly.

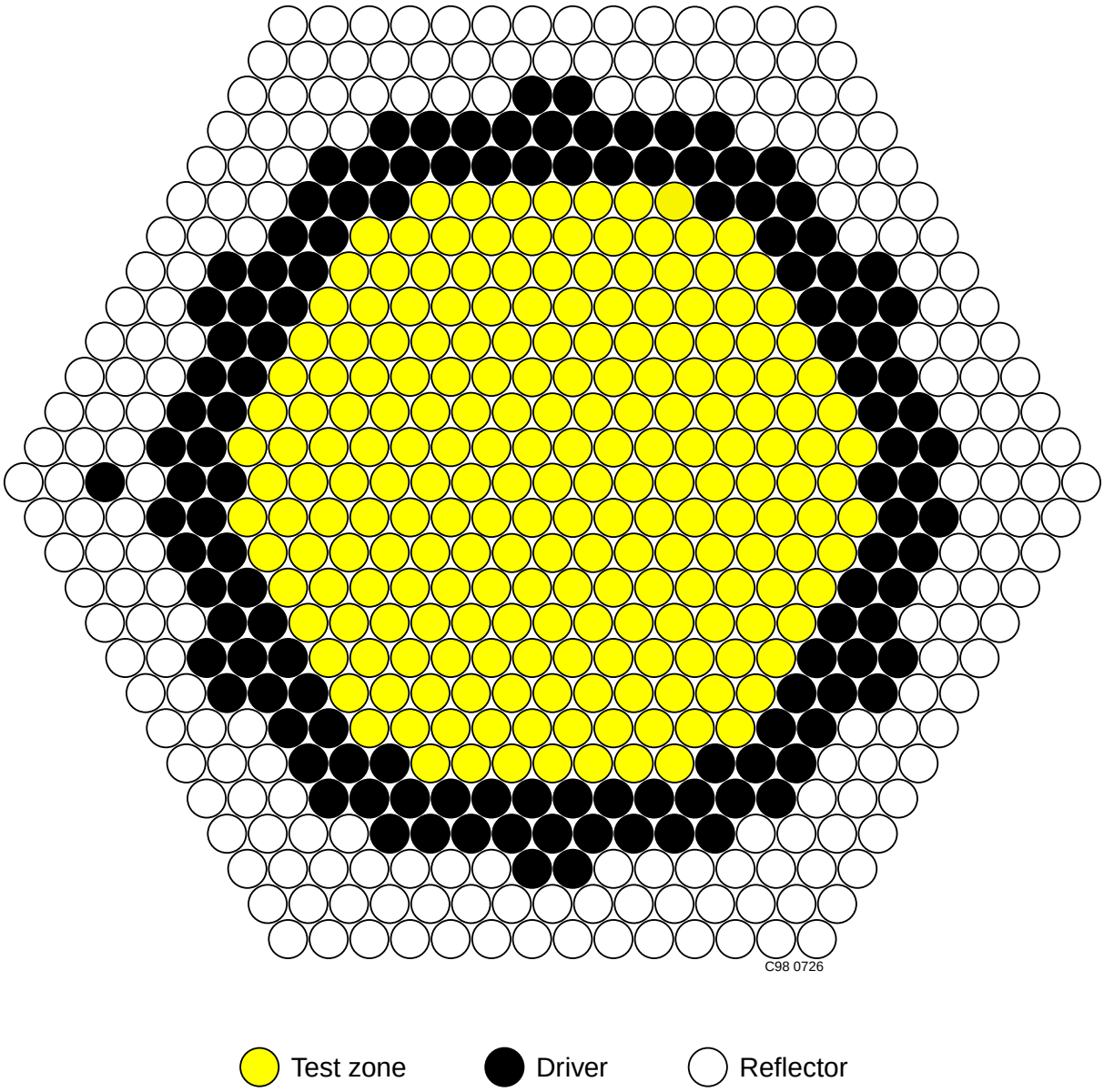

Figure 5. The Loading Diagram of the KBR-9 Critical Assembly.

KBR-10 ASSEMBLY

On the whole, construction of the KBR-10 assembly is the same as KBR-9. Compositions of unit cells and loading of fuel rods are represented in Figure 6. In Figure 7 the layout of the assembly is shown.

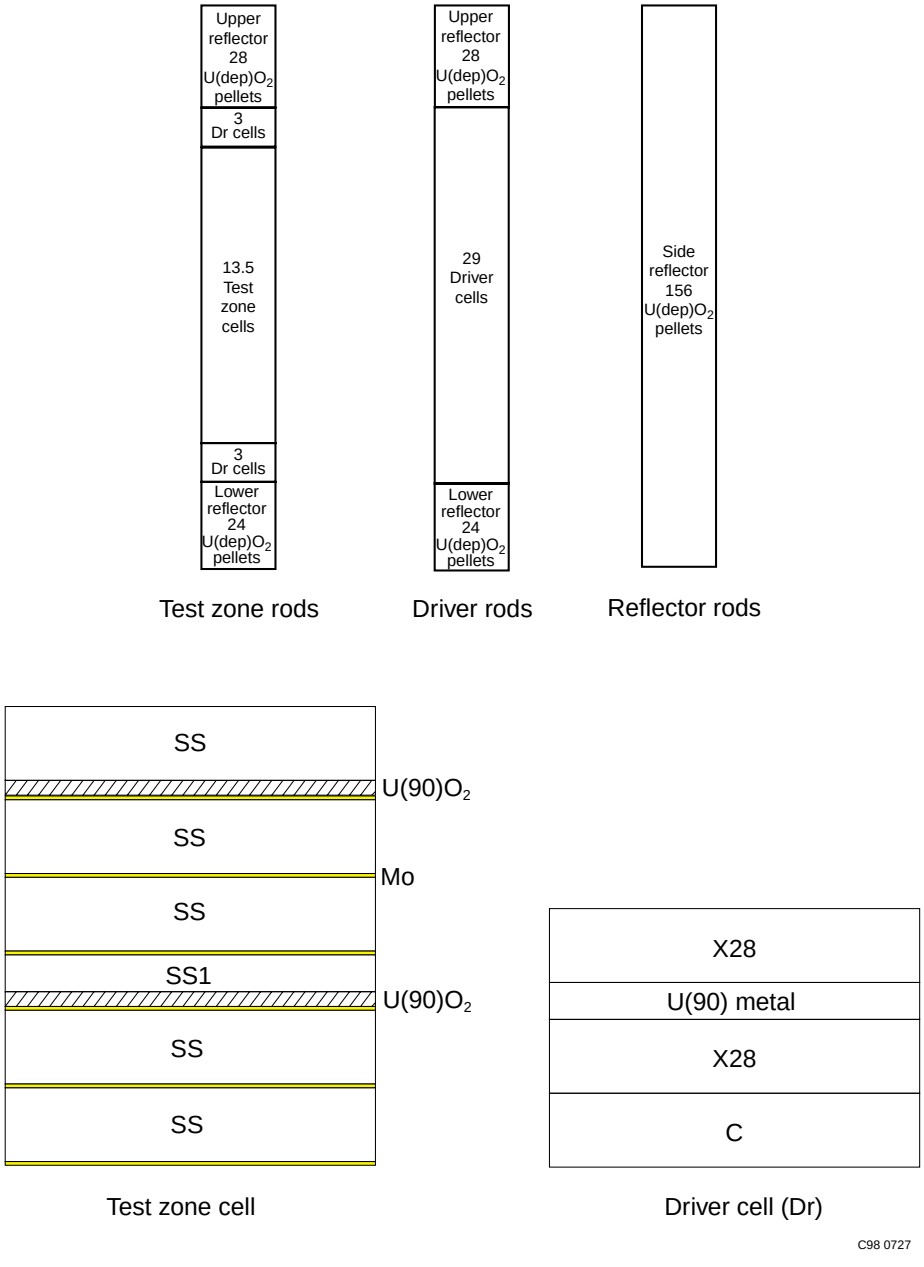

Figure 6. Compositions of Unit Cells and Fuel Rods of the KBR-10 Assembly.

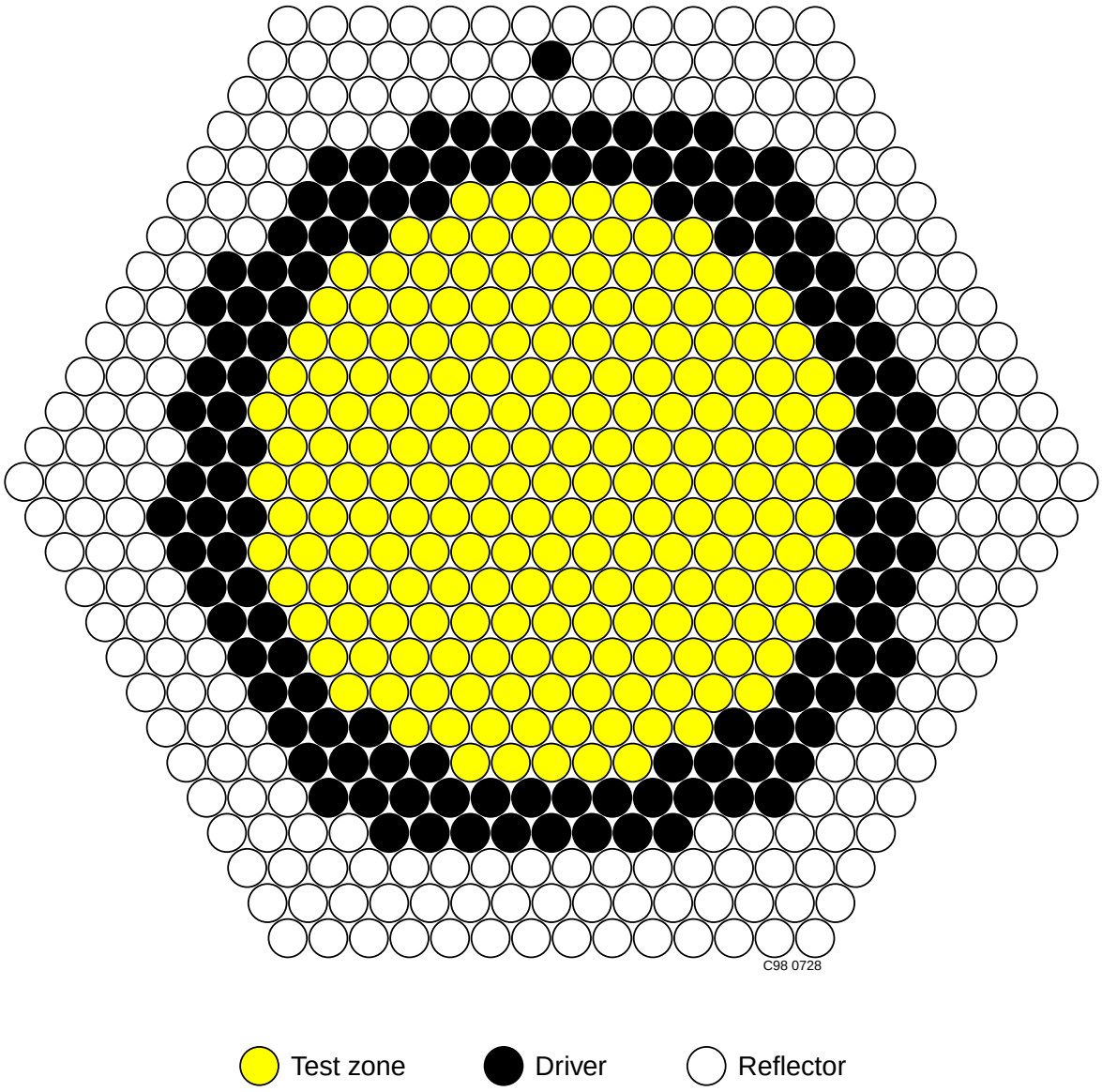

Figure 7. The Loading Map of the KBR-10 Assembly.

KBR-15 ASSEMBLY

Construction of the KBR-15 assembly was the same as KBR-9 and KBR-10 except that the upper, lower, and radial intermediate zones consisting of uranium dioxide and steel X28 pellets were added. Compositions of unit cells of different zones and loading of fuel rods are shown in Figure 8. The layout of assembly KBR-15 is represented in Figure 9.

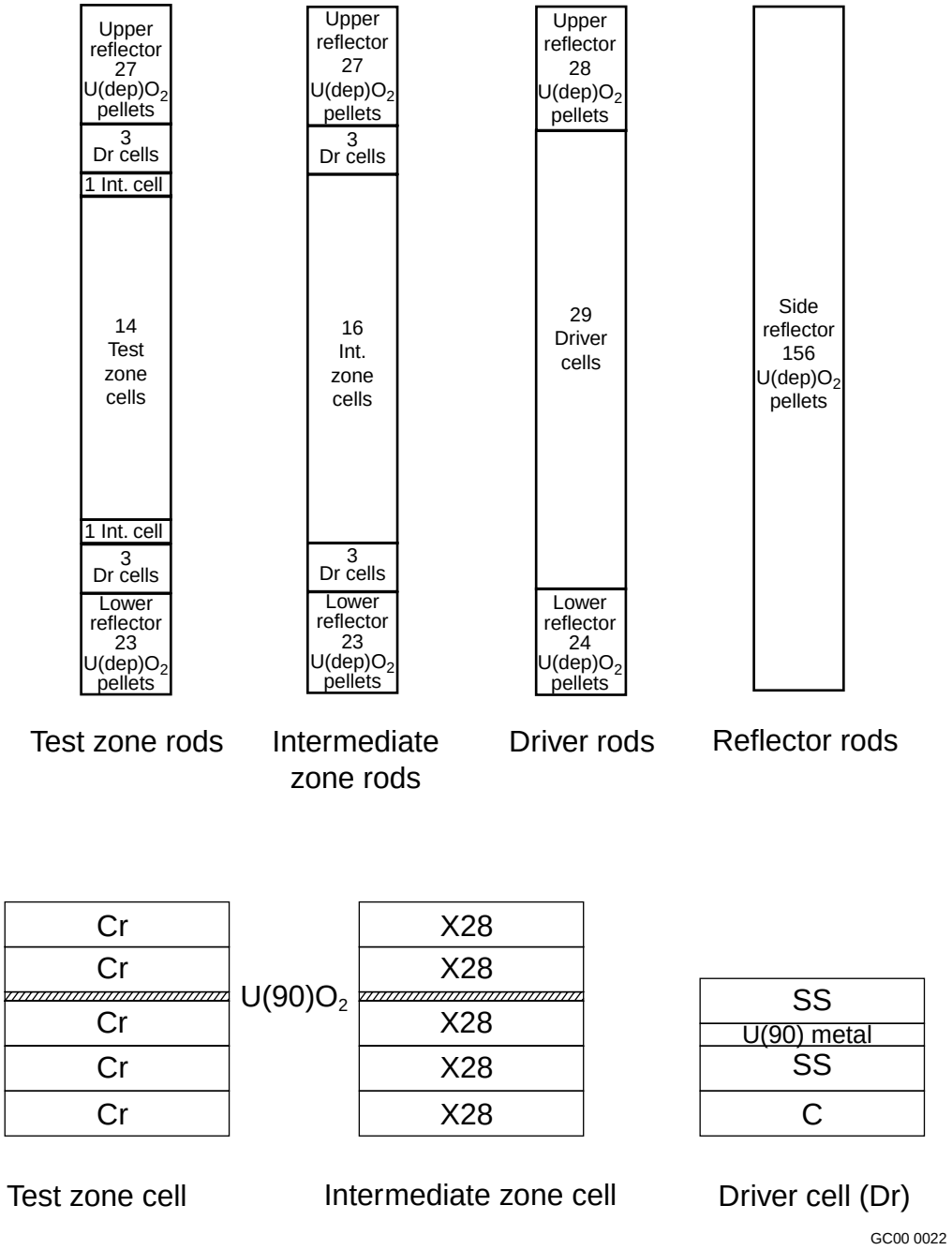

Figure 8. Compositions of Fuel Rods and Unit Cells of the KBR-15 Assembly.

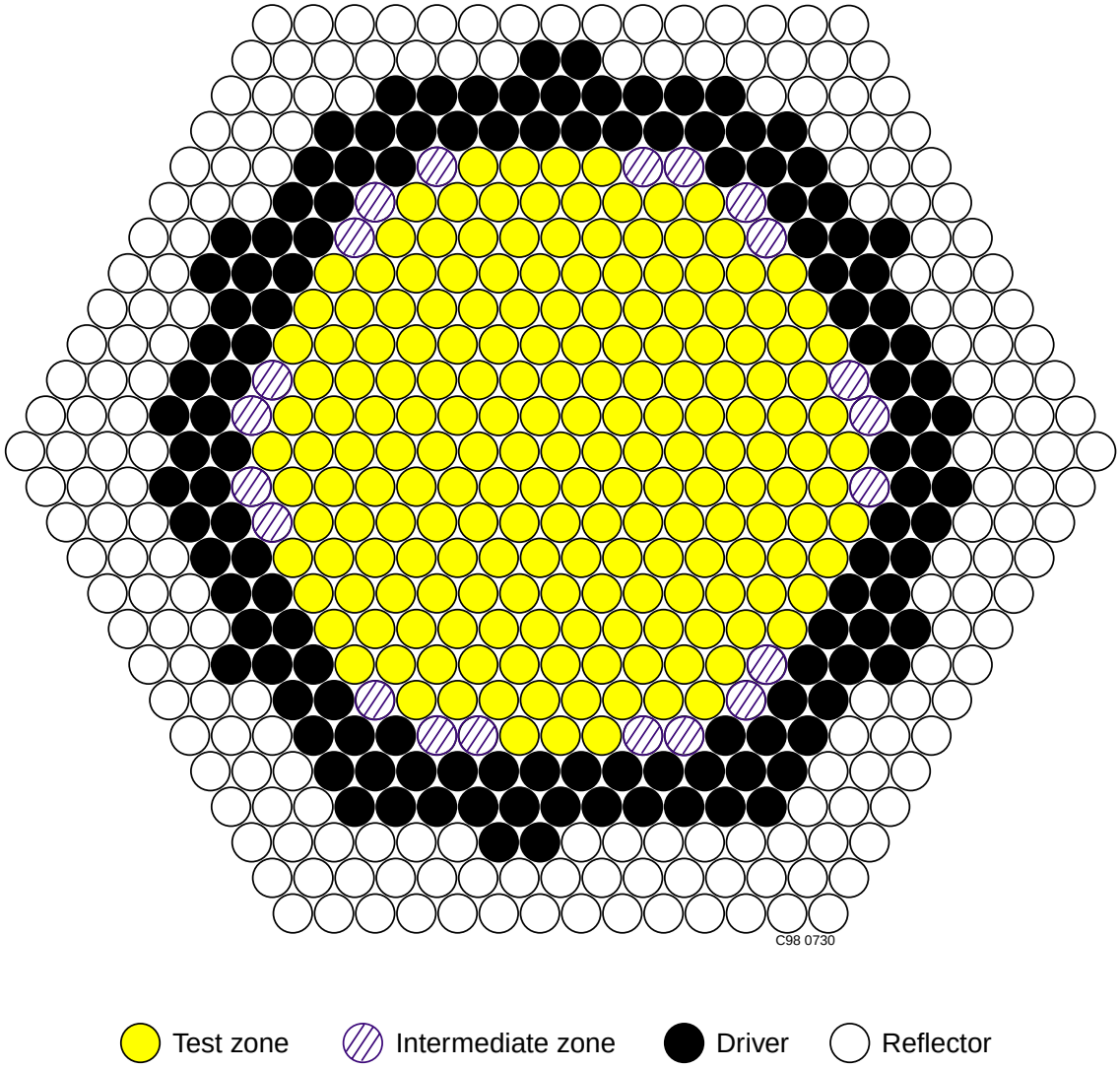

Figure 9. The Layout of the KBR-15 Assembly.

KBR-16 ASSEMBLY

Compositions of different zones' unit cells and loading of fuel rods are shown in Figure 10. The layout of the KBR-16 critical assembly is represented in Figure 11.

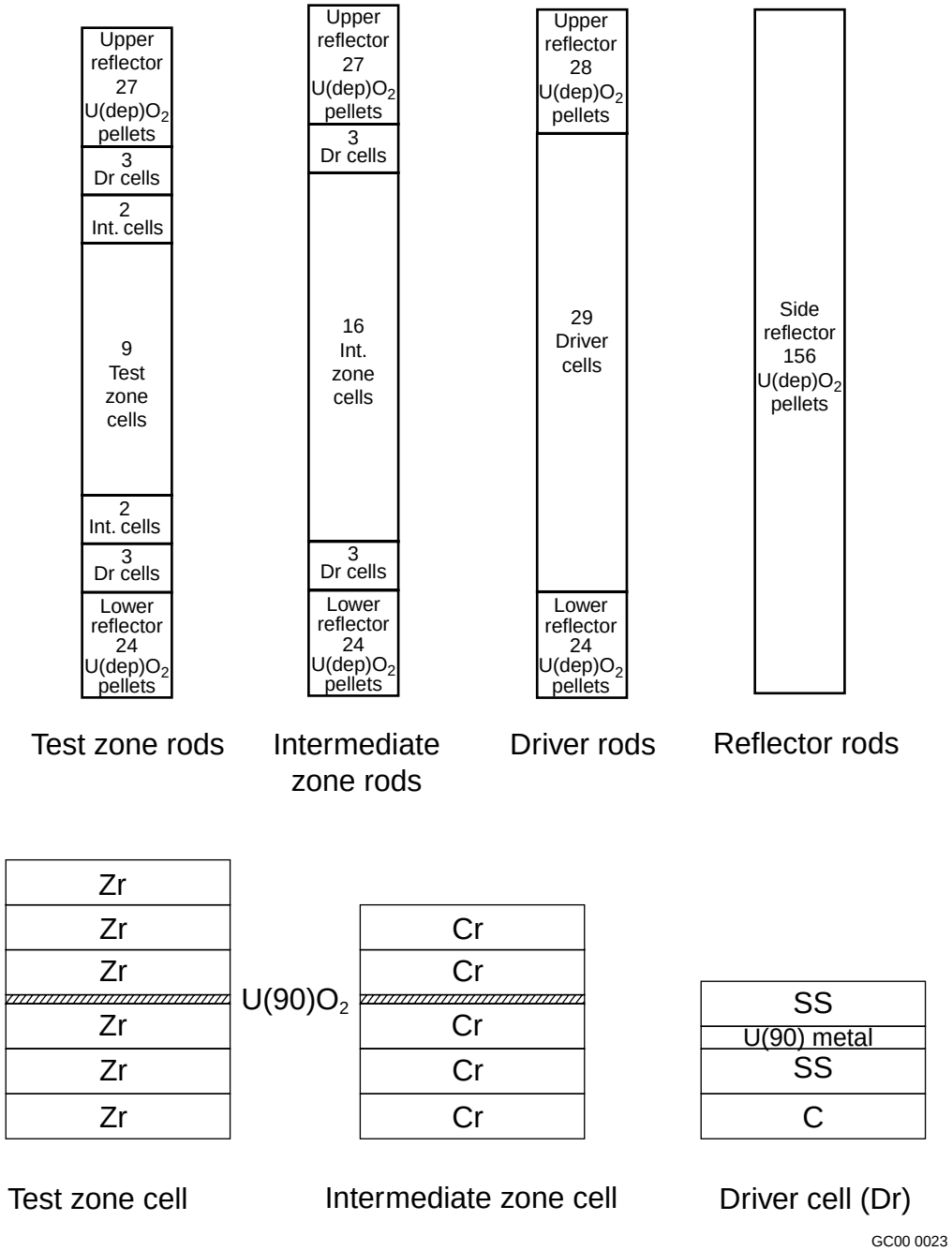

Figure 10. View of Rods and Unit Cells of the Various Zones of the KBR-16 Assembly.

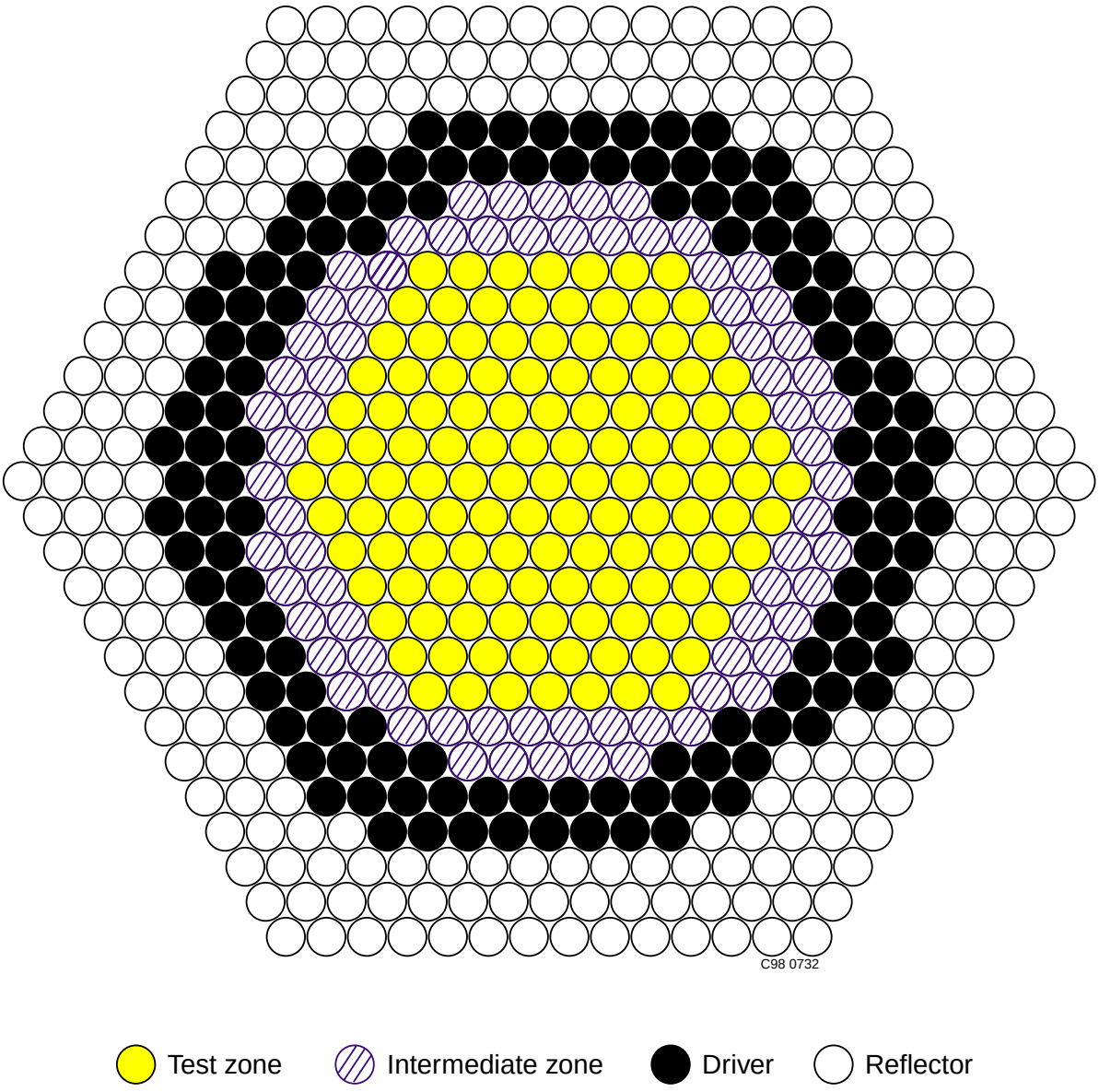

Figure 11. The Layout of the KBR-16 Assembly.

5. SUPPLEMENTAL EXPERIMENTAL MEASUREMENTS

Ratios of the reactivity worths of structural materials to reactivity worth of ^{235}U were measured in the center of each assembly in the cavity formed by the extraction of the central cell of the lattice from the stainless steel container (see Section 4). Measurements were performed using sample pellets of different thicknesses. Sample pellets were installed in the center of the cavity with the help of two thin stainless steel rings (see Figure 12). Final results were obtained by extrapolation of data to zero thickness of the sample pellet. Uncertainties of data shown below include uncertainties of the extrapolation.

For the materials not contained in the test region cell (such as Fe or Ni in KBR-15) or contained in small concentration (Ni in KBR-10 for example), the measured reactivity worth is partly caused by reduced resonance self-shielding in the surrounding cells due to neutron scattering in the sample. For thick samples, resonance self-shielding of cross sections in the sample is also important. The last effect goes to zero as sample thickness is reduced faster than the reactivity caused by neutron absorption and slowing down in the sample. Thus it could be eliminated by extrapolation of measured reactivity worth (reactivity of the sample divided by the weight of sample expressed in the moles) to zero thickness. But the effect of reduced resonance self-shielding in the surrounding cells goes to zero at approximately the same rate as absorption and slowing-down effects and thus cannot be eliminated by extrapolation. If this measured reactivity-worth data would be compared with calculated ones, the last effect must be taken into account.

Due to self-shielding, extrapolation to zero thickness leads to additional uncertainty for materials not contained in the surrounding media. For the main structural materials, cross-section self-shielding in the sample and hence measured reactivity worth do not depend on the thickness of the sample (Ni sample in KBR-7, Cr sample in KBR-15) or depend so little on it (Fe in KBR-10) that extrapolation to zero thickness does not lead to additional uncertainty. So uncertainties of measured reactivity worth of the main structural materials are relatively small.

Samples of highly enriched uranium were used as the reactivity-worth standard. Contributions of ^{238}U were extracted using results of measurements with samples of depleted-uranium.

Reactivity worths were determined as the reactivity per mole of material. In Table V ratios of reactivity worths of materials shown in the first column to reactivity worth of ^{235}U are shown.

Table V. Reactivity-Worth Ratios Measured in the Centers of Assemblies (multiplied by 10^3).

Material	KBR-7 (Ni)	KBR-9 (St. Steel)	KBR-10 (St. Steel & Mo)	KBR-15 (Cr)	KBR-16 (Zr)
Iron	-5.0 ± 0.2	-3.4 ± 0.1	-3.3 ± 0.1	-4.3 ± 0.2	-5.6 ± 0.2
Chromium	-5.5 ± 0.3	-4.8 ± 0.3	-5.3 ± 0.3	-2.6 ± 0.1	-6.3 ± 0.3
Nickel	-6.2 ± 0.1	-8.9 ± 0.2	-10.3 ± 0.3	-12.1 ± 0.4	-14.0 ± 0.4
Zirconium	-	-	-	-	-5.7 ± 0.2

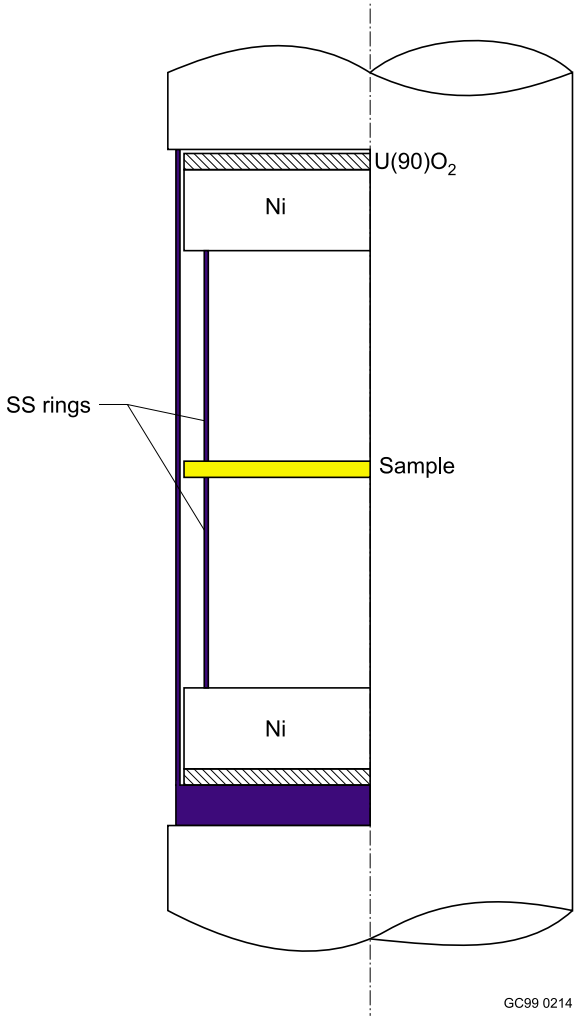

Figure 12. Arrangement of Sample for Reactivity-Worth Measurement in the Cavity Formed by Removal of the Central Cell (example for KBR-7 cell as in Section 4). Thickness of the Stainless Steel Spacing Rings is 0.02 cm.

6. RESULTS OF CALCULATIONS

k_∞ was estimated as[2]

$$k_\infty \cong k_{\infty,\exp} = \frac{R}{1-(\rho_{cell}/\rho_{fuel})\times f}$$

where R and f are calculated correction factors.[1,2]

One-dimensional slab models of the test cells were developed to calculate estimates of the uncertainties of the correction factors and measurements. The FFCP[3] code with the ABBN-93[4]

cross-section set was used with the slab model of the cell and collision probability method to prepare homogenized group cross sections, flux-averaged over the cell for assembly calculations. The CRAB-1[5] code, using the prepared homogenized group cross sections, was used for neutronics calculations with the S_8 discrete-ordinates method and transport-corrected P_0 cross sections.

Uncertainties were estimated[1] taking into account the following independent sources:

1. uncertainty of the neutron data (using covariance matrices of the ABBN-93 system);
2. uncertainty of cell composition (using data of composition uncertainties);
3. uncertainty of the heterogeneity treatment (estimated, using the FFCP calculations, for capture and fission cross sections as 30% of the total heterogeneity effect and for the transport cross section as 100% of the total heterogeneity effect);
4. uncertainty of the 26-group approximation (estimated as the difference between results of calculations using 299 groups and using 26 groups collapsed from them);
5. uncertainty of the assembly geometry treatment (estimated as half the difference between results of three-dimensional and one-dimensional calculations of *R*);
6. uncertainty of the ρ_{cell}/ρ_{fuel} measurement (Table I).

Evaluated k_∞'s and uncertainties for unit cells in Figure 1 at hexagonal pitch 5.1 cm and calculated results using different codes and cross sections are given in the following tables. There are large (up to 15%) discrepancies between the evaluated experimental results and the calculations, as well as between the different codes and cross sections.

Table VI. Experimental k_∞'s and Sample Calculation Results (Russian Federation Cross Sections).

Configuration	Experimental k_∞ and Uncertainty	KENO (ABBN-93)	Calculated Result/ Experimental Measurement
KBR-7 (Ni)	1.032 ± 0.004	1.0157 ± 0.0003	0.984
KBR-9 (St. Steel)	1.050 ± 0.008	1.0779 ± 0.0004	1.027
KBR-10 (St. Steel & Mo)	1.030 ± 0.006	1.0354 ± 0.0004	1.005
KBR-15 (Cr)	1.064 ± 0.018	1.1141 ± 0.0003	1.047
KBR-16 (Zr)	0.997 ± 0.013	0.9457 ± 0.0004	0.949

Table VII. Sample Calculation Results (United States Codes and Cross Sections).

Code (Cross Section Set) → Configuration ↓	MCNP (Continuous-Energy ENDF/B-V)	Calculated Result/ Experimental Measurement	MCNP (Continuous-Energy ENDF/B-VI)	Calculated Result/ Experimental Measurement
KBR-7 (Ni)	0.9920 ± 0.0004	0.961	1.0368 ± 0.0004	1.005
KBR-9 (St. Steel)	1.0344 ± 0.0004	0.985	1.1121 ± 0.0004	1.059
KBR-10 (St. Steel & Mo)	0.9887 ± 0.0004	0.960	1.0445 ± 0.0004	1.014
KBR-15 (Cr)	0.9020 ± 0.0004	0.848	1.1636 ± 0.0004	1.094
KBR-16 (Zr)	0.8708 ± 0.0004	0.873	0.9484 ± 0.0004	0.951

Table VIII. Sample Calculation Results (United States Codes and Cross Sections, cont'd).

Code (Cross Section Set) → Configuration ↓	KENO (238-Group ENDF/B-V)	Calculated Result/ Experimental Measurement	KENO (44-Group ENDF/B-V)	Calculated Result/ Experimental Measurement
KBR-7 (Ni)	0.9808 ± 0.0003	0.950	0.9819 ± 0.0004	0.951
KBR-9 (St. Steel)	1.0239 ± 0.0003	0.975	1.0168 ± 0.0003	0.968
KBR-10 (St. Steel & Mo)	--	--	--	--
KBR-15 (Cr)	0.9598 ± 0.0004	0.902	0.8802 ± 0.0004	0.827
KBR-16 (Zr)	0.9717 ± 0.0004	0.975	0.9802 ± 0.0004	0.983

Calculated spectral data for the five test regions are shown in Tables IX and X and in Figure 13.

Table IX. Spectral Characteristics of the Experiments.

Case Number	EALF[a], eV	AFGE[b], EV	Flux, %		
			< 0.625 eV	0.625 eV - 100 keV	> 100 keV
KBR-7	5.12E+3	4.63E+3	0.0	38.0	62.0
KBR-9	3.59E+3	3.36E+3	0.0	50.3	49.7
KBR-10	7.21E+3	6.64E+3	0.0	48.3	51.7
KBR-15	4.40E+3	4.09E+3	0.0	56.8	43.1
KBR-16	4.14E+3	3.90E+3	0.0	55.7	44.3

[a] Energy corresponding to the average lethargy of neutrons causing fission.
[b] Energy corresponding to the average energy group of neutrons causing fission.

Table X. Spectral Characteristics of the Experiments.

Case Number	Fission, %			Capture, %		
	< 0.625 eV	0.625 eV - 100 keV	> 100 keV	< 0.625 eV	0.625 eV - 100 keV	> 100 keV
KBR-7	0.1	71.2	28.7	0.1	63.4	36.6
KBR-9	0.0	79.4	20.6	0.0	83.6	16.3
KBR-10	0.0	75.2	24.7	0.0	82.1	17.9
KBR-15	0.0	82.3	17.7	0.0	84.9	15.1
KBR-16	0.2	81.5	18.3	0.1	88.6	11.3

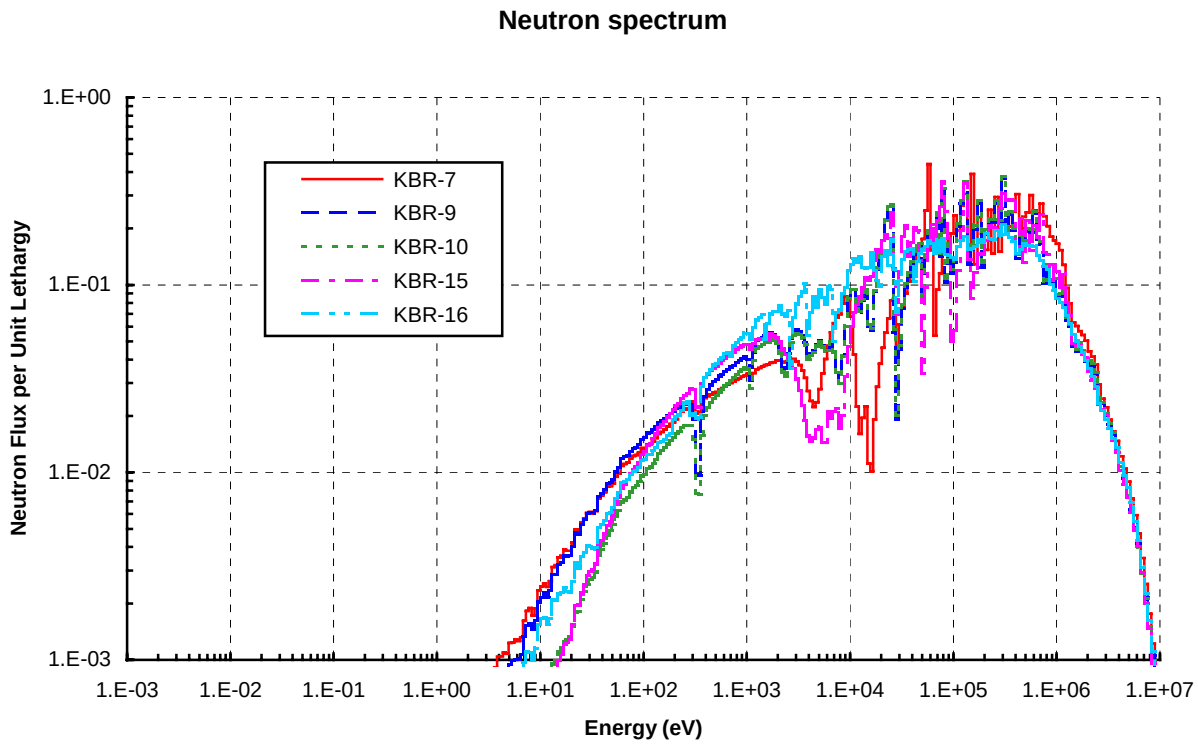

Figure 13. Calculated Neutron Spectra.

These experiments were especially designed to test the cross sections of the structural materials and they are highly sensitive to these cross sections. It is easy to see from the neutron balance table (Table XI) that neutron captures in structural materials in all cases make a large contribution to the whole neutron absorption. This indicates that differences in these cross sections are the main reason for discrepancies in the results of different calculations.

Table XI. Balance of Fissions and Captures by Isotopes over the Core.

	Isotope	KBR-7 (Ni)	KBR-9 (SS)	KBR-10 (SS+Mo)	KBR-15 (Cr)	KBR-16 (Zr)
Percent of Fissions	^{235}U	41.4	44.0	42.3	45.6	38.6
Percent of Captures	^{235}U	14.1	15.7	14.1	15.8	13.6
	^{238}U	1.5	1.7	1.2	1.4	1.3
	Fe	1.4	18.8	14.7	2.9	2.8
	Cr	0.5	7.2	5.7	32.3	1.2
	Ni	39.1	6.7	5.7	1.0	1.0
	Mn	0.4	5.4	4.0	0.9	0.8
	Ti	--	0.4	0.3	--	--
	Co	1.5	--	--	--	--
	Zr	--	--	--	--	39.6
	Hf	--	--	--	--	1.0
	Mo	--	--	11.9	--	--
$\nu\Sigma_f/\Sigma_a$		1.02	1.08	1.04	1.11	0.95

For example, comparison of self-shielded chromium capture cross sections in the ABBN-93 library and in the 238-group ENDF/B-V library show that in the energy region above 10 keV, the latter exceed the former by as much as three to five times. Thus the evaluated integral data presented here can be used to select the more reliable among different cross-section sets, and to indicate regions needing improvement in others.

CONCLUSIONS

The experiments presented here were especially designed to test the cross sections of the structural materials and they are highly sensitive to these cross sections. There are several large discrepancies between the experimental results and the calculations performed using different codes and cross-sections. Thus these experiments provide a valuable test for checking the cross sections of the considered structural materials.

REFERENCES

1. *International Handbook of Evaluated Criticality Safety Benchmark Experiments*, NEA/NSC/DOC(95)03/I-VII, OECD-NEA, Vol II, HEU-COMP-INTER-005 (September 1999 Edition).

2. M. Nakano, T. Iijima, "Interpretation of the Central Cell Reactivity Worth and Experimental Determination of a Characteristics Value of the Reactor Cell Composition K^+m," *Journal of Nuclear Science and Technology*, **10**(2), pp. 69-79 (February 1973).

3. A. A. Bezborodov, B. G. Ryazanov, M. M. Savos'kin, “Calculations of Heterogeneous Effects in Cores of Fast Critical Assemblies with First-Flight Collision Probability Method,” *VANT, Ser. Physics and Engineering of Nuclear Reactors*, **2**, p. 8 (1986)

4. RSICC Data Library Collection, “DLC-182: ABBN-93 – Multigroup Constant Set for Calculation of Neutron and Photon Radiation Fields and Functionals, Including the CONSYST2 Program.”

5. M. M. Savos’kin, M. A. Baryba, A. A. Bezborodov, et al., “Annotation of the CRAB-1 Code,” *VANT, Ser. Physics and Engineering of Nuclear Reactors*, **6**, p. 43 (1984)